drones

MDPI

Article

Sensing-Assisted UAV-BS Recovery for Invisible Evacuee Demand Along Predefined Evacuation Corridors

Weichao Yang [1], Yuqing Lu [1], Dawei Wang [1,*], Yixin He [2], Yi Jin [1] and Li Li [1]

[1] School of Electronics and Information, Northwestern Polytechnical University, Xi'an 710129, China; yangwc@nwpu.edu.cn (W.Y.); luyuqing@mail.nwpu.edu.cn (Y.L.); yinyi@nwpu.edu.cn (Y.J.); lil@nwpu.edu.cn (L.L.)
[2] College of Information Science and Engineering, Jiaxing University, Jiaxing 314001, China; yixinhe@zjxu.edu.cn
* Correspondence: wangdw@nwpu.edu.cn

Highlights

What are the main findings?

- A sensing-assisted UAV-BS recovery model is developed for predefined evacuation corridors under ground coverage and network observation blind zones.
- The proposed invisible-demand map and evacuation-flow demand map jointly capture evacuee demand that is invisible to the surviving network and communication continuity along evacuation corridors.

What are the implications of the main findings?

- The proposed method shifts post-disaster UAV-BS deployment from network-side visible metrics or responses based on coverage degradation toward aerial network recovery guided by constructed demand maps.
- The demand-map representation provides an effective way to incorporate aerial sensing information into UAV-BS recovery decisions under limited network observability.

Abstract

Post-disaster emergency communication networks often suffer from coverage degradation and limited network observability, which makes it difficult to maintain reliable connectivity for evacuees. Existing UAV-assisted communication methods usually rely on network-side visible metrics for deployment decisions. As a result, they may overlook evacuees whose communication demands are hidden in coverage blind zones or observation blind zones along predefined evacuation corridors. To address this problem, this paper proposes a sensing-assisted UAV-BS recovery method for invisible evacuee demand. The method constructs an invisible-demand map by combining sensed evacuee states, ground coverage conditions, network observation states, and evacuation urgency. It further introduces an evacuation-flow demand map to describe continuous communication demand along evacuation corridors. These two maps are combined to guide temporary UAV-BS access recovery. The simulation results show that the proposed method achieves the best overall balance among invisible-demand recovery, evacuation-path coverage, and edge evacuee rate. Compared with the blind-zone-only baseline, it improves DCR (demand coverage ratio) from 0.365 to 0.373, DW-EPC (demand-weighted evacuation-path coverage) from 0.286 to 0.316, and the fifth-percentile evacuee rate from 1.559 to 1.672 bps/Hz. The proposed method also shows more stable performance under sensing-output uncertainty and constrained UAV response radius.

Academic Editor: Emmanouel T. Michailidis

Received: 25 May 2026
Revised: 28 June 2026
Accepted: 1 July 2026
Published: 3 July 2026

 https://doi.org/10.3390/drones10070507

Keywords: UAV-BS; post-disaster emergency communication; predefined evacuation corridor; aerial network recovery; invisible-demand map; observation blind zone

1. Introduction

With accelerating urbanization and high population concentration, sudden disasters, such as earthquakes, floods, and fires, can significantly impact urban operations and public safety. Consequently, disaster emergency response has become increasingly important [1]. Post-disaster environments are highly dynamic, and evacuation status and road conditions are often difficult to monitor in real time. Timely information feedback and command coordination are therefore essential for emergency response [2]. However, this information chain may be weakened by base station failures and power limitations, which degrade ground network performance and reduce link reliability. Therefore, communication support directly affects evacuation efficiency and rescue coordination.

In post-disaster evacuation scenarios, communication support must facilitate continuous information exchange rather than simply restore static network coverage. Evacuees typically move toward safe zones along predefined paths, which form critical evacuation corridors [3–5]. Because information exchange is concentrated along these corridors, they become priority areas for emergency communication support. When ground network coverage degrades, evacuees moving along these routes may face disconnection risks, which can hinder evacuation organization [6]. Therefore, communication recovery for predefined evacuation corridors must provide continuous service that adapts to dynamic demand.

To meet these requirements, relying solely on ground base station repairs or the deployment of temporary ground equipment is often insufficient. Ground-based recovery is limited by environmental complexity, blocked roads, and restricted power supplies [7,8]. In contrast, a UAV-mounted base station (UAV-BS) can be rapidly deployed to create a temporary aerial access point, providing communication service to evacuees who are difficult to serve through damaged ground networks [9,10]. Furthermore, the three-dimensional mobility and coverage reconfiguration capabilities of the UAV-BS enable it to adjust its service position within a limited operational radius based on demand changes near the corridor, providing mobile aerial support for communication recovery along predefined evacuation corridors [11]. Beyond this limited operational radius, UAV-assisted emergency communication is also constrained by onboard energy. Recent advances in low-power design, energy harvesting, and intelligent power management improve platform autonomy [12] and offer ways to extend operation when ground power infrastructure is unavailable [13].

However, the effectiveness of UAV-BS deployment depends not only on aerial coverage capability but also on whether the system can identify communication demands that should be restored with priority. The existing studies mostly determine service locations from already connected users, visible traffic hotspots, or detectable coverage-degraded regions [14,15], so the aerial service may be biased toward observable hotspots while overlooking disconnected evacuee demand that is invisible to the surviving network. For predefined evacuation corridors, this invisible demand arises from two distinct types of ground-network degradation, which we refer to as coverage blind zones and observation blind zones.

In real disaster scenarios, these two types arise from different physical causes and should be distinguished. A coverage blind zone reflects a loss of service capability, where the signal quality from the surviving base stations falls below a usable threshold, whereas an observation blind zone reflects a loss of demand visibility, where the surviving network cannot detect present users or communication requests even at locations whose nominal coverage is not fully lost. The two need not coincide: a congested or partially functional area may still appear served on network-side coverage maps while many disconnected evacuees remain invisible to it, and a recovery decision based only on coverage degradation would overlook them.

This motivates a recovery framework that converts sensing outputs into spatial demand maps for UAV-BS position selection. In this paper, aerial network recovery refers to restoring access-side communication service for prioritized evacuee demand by selecting the UAV-BS position in each decision period rather than repairing the ground infrastructure or the backhaul. The invisible-demand map is a spatial field that indicates where evacuee communication demand exists but cannot be reliably served or observed by the surviving ground network, while the evacuation-flow demand map is a spatial field that indicates the continuous and directional communication demand generated by evacuees moving along the predefined corridor. Recent sensing-assisted and ISAC studies show that sensing outputs can support wireless decision making beyond conventional communication-side measurements [16–18]. Based on these maps, we develop demand-weighted criteria for selecting UAV-BS recovery positions and determine the recovery position using a lightweight adaptive position search algorithm guided by the constructed demand maps.

The main contributions of this paper are summarized as follows:

- We formulate a sensing-assisted aerial network recovery framework for predefined evacuation corridors. In this framework, coverage blind zones and observation blind zones are distinguished to describe two types of ground-network degradation: weak service capability and poor demand visibility. This distinction provides the basis for modeling invisible communication demand.
- We construct an invisible-demand map and an evacuation-flow demand map. Evacuee states obtained from aerial sensing are used to describe the spatial distribution of underlying communication demand. Ground coverage degradation, network observation degradation, and corridor relevance are then combined to generate the invisible-demand map, while the evacuation-flow demand map captures continuous communication needs caused by crowd movement along predefined corridors.
- We develop a demand-weighted UAV-BS aerial network recovery criterion. This criterion links UAV-BS position selection with invisible-demand recovery and communication continuity along the evacuation flow. A lightweight adaptive position search algorithm guided by the constructed demand maps is then used to find the UAV-BS recovery position within a limited response range.

The remainder of this paper is organized as follows. Section 2 reviews the related studies on UAV-assisted post-disaster communication, recovery based on coverage degradation, density-aware UAV-BS deployment, sensing-assisted communication, and the spatial structure of evacuation routes. Section 3 develops the system model for the scenario with predefined evacuation corridors, including the damaged terrestrial network, evacuee state, coverage blind zone, observation blind zone, and UAV-BS aerial service model. Section 4 formulates the invisible-demand map based on sensing outputs and the evacuation-flow demand map and then constructs the demand-weighted aerial network recovery criterion and the adaptive position search method. Section 5 presents the simulation settings and results, comparing different UAV-BS deployment criteria in terms of invisible-demand coverage, disconnected-user recovery, evacuation-path coverage, and edge evacuee rate. Section 6 concludes the paper and discusses future extensions.

2. Related Work

2.1. UAV-BS Support for Post-Disaster Communication Recovery

When disasters cause base station failures, backhaul blockage, or local service interruption, the ground network may not be able to provide timely communication support. UAV-BSs provide an aerial means of emergency service recovery. Owing to fast deployment and flexible positioning, they can serve as temporary access nodes before the terrestrial infrastructure is fully repaired.

The existing studies have built a solid foundation for post-disaster communication recovery supported by UAV-BSs. UAV-BS deployment under failed base stations and non-uniform user distributions has been studied to restore service coverage, message delivery, and rescue connectivity [10,11,19]. More recently, Pijnappel et al. studied online positioning of a drone-mounted base station under site failures and traffic hotspots, showing that UAV-BS positions should adapt to post-disaster network states [14]. Related UAV trajectory and coverage-optimization studies in mobile edge computing and wireless-powered IoT systems typically optimize UAV motion under known or observable task demands [20,21]. In contrast, this paper focuses on post-disaster UAV-BS recovery when part of the evacuee demand is hidden from the surviving network. Beyond positioning, complementary physical-layer studies on secure transmission, rate-splitting multiple access, and RIS-assisted aerial communication have further enriched aerial emergency networks [22–25].

These studies demonstrate the feasibility of using UAV-BSs as aerial compensation nodes. Nevertheless, existing UAV-BS positioning methods mostly determine service locations from visible network states, modeled user distributions, or detectable service gaps. In predefined evacuation corridors, the most critical communication demand may come from evacuees who are moving but disconnected from the surviving network, which is difficult to infer from cellular-side measurements alone. Therefore, beyond optimizing UAV-BS locations, it is also necessary to construct a spatial representation of recovery demand that reveals where emergency communication recovery is actually needed.

2.2. Spatial Information for UAV-BS Deployment

The effectiveness of UAV-BS deployment depends strongly on the spatial information used to guide the aerial service position. The existing studies provide useful references from four perspectives: ground coverage state, user demand distribution, external sensing information, and the spatial structure of evacuation routes.

The first perspective is the ground coverage state. Coverage-hole recovery studies usually identify areas where the received signal quality is below a service threshold and then deploy UAV-BSs to compensate for these service gaps. Al-Ahmed et al. considered autonomous coverage-hole detection, wireless backhaul, and user demand in UAV-BS placement, showing that detected service gaps can provide a direct basis for aerial compensation deployment [15]. This line of work is closely related to the coverage degradation considered in this paper. However, a coverage gap only describes whether a location can be served. It does not indicate whether the surviving network can observe the demand at that location.

The second perspective is user demand distribution. Hotspot-driven and density-aware methods move UAV-BSs toward areas with concentrated users or high traffic demand. Lai et al. studied on-demand density-aware UAV-BS placement for arbitrarily distributed users with guaranteed data rates, indicating that user density is an important reference for UAV-BS deployment [26]. Such methods are effective when user demand is known or can be reliably estimated by the network. In post-disaster evacuation scenarios, however, disconnected evacuees may not generate stable network-side measurements.

The third perspective is external sensing. Integrated sensing and communication (ISAC) and sensing-assisted communication studies show that radar, vision, or other sensors can provide target locations, environmental states, or localization information beyond conventional network-side measurements [16–18]. Recent UAV-ISAC studies have further considered trajectory design, beamforming, resource allocation, and sensing-quality constraints in different emergency or IoT scenarios [27–29]. These studies confirm the value of sensing information for wireless systems. However, they mainly treat sensing as an objective or constraint rather than as a source of recovery demand for evacuees who are invisible to the surviving network. In this paper, sensing outputs are used at the system-output layer to complement network-side observations and support UAV-BS recovery decisions.

The fourth perspective comes from studies of evacuation routes and crowd movement. Pedestrian evacuation studies have modeled exit corridors as structured evacuation spaces [30]. Evacuation path planning studies under fire scenarios further show that evacuation demand has strong spatial directionality [31]. UAV-based evacuation guidance systems also demonstrate that aerial platforms can support evacuation services along planned routes when ground information is limited [32]. These works do not address communication recovery, but they show that predefined evacuation routes should be treated as important spatial structures in emergency systems.

Table 1 summarizes the design-level differences between representative UAV-BS recovery studies and the proposed method. The existing designs provide useful foundations from different angles, but most of them rely on visible network states, coverage conditions, known user density, or sensing-quality objectives. They do not explicitly distinguish service loss from demand invisibility, nor do they connect sensing-revealed evacuee states with evacuation-flow continuity. Motivated by these gaps, this paper constructs recovery-oriented demand maps for UAV-BS aerial network recovery in predefined evacuation corridors.

Table 1. Comparison with representative UAV-BS deployment and sensing-assisted recovery designs.

Representative Design	Main Information Used	Main Missing Issue	This Work
Network-visible or demand-aware UAV-BS deployment [9,14,19]	Visible traffic demand, user distribution, service state, and UAV position	Network-invisible evacuees may be missed	Uses sensing-revealed evacuee states to expose invisible demand
Coverage- or density-aware UAV-BS placement [15,26]	Coverage condition, user density, target rate, and UAV altitude	Service loss and demand invisibility are not distinguished	Separates coverage and observation blind zones
UAV-assisted ISAC or sensing-assisted deployment [16–18]	Sensing quality, communication rate, trajectory, and resource allocation	Treats sensing mainly as an objective or constraint	Uses sensing outputs as recovery demand inputs
UAV-assisted evacuation design [3]	Evacuation route, crowd state, and guidance information	Focuses on guidance rather than communication recovery	Adds evacuation-flow demand for corridor communication continuity
Proposed design	Sensed evacuee state, network degradation, corridor relevance, and evacuation flow	–	Integrates invisible-demand and evacuation-flow continuity for UAV-BS recovery position selection

3. System Model

3.1. Post-Disaster Network Scenario Modeling and Predefined Evacuation Corridor

We consider a post-disaster emergency communication scenario, as illustrated in Figure 1. In this scenario, a UAV-BS provides temporary aerial service for disconnected evacuees moving along a predefined evacuation corridor in the presence of ground coverage blind zones and network observation blind zones. The affected area is modeled as a two-dimensional plane $\mathcal{A} \subset \mathbb{R}^2$. After the disaster, the ground infrastructure is represented by a set of surviving and failed base stations. Let $\mathcal{B}$ denote the set of ground base stations deployed in the area before the disaster. The base stations are then divided into a surviving set $\mathcal{B}_g$ and a failed set $\mathcal{B}_f$, where $\mathcal{B}_g = \{1, 2, \ldots, B\}$, and B is the number of surviving ground base stations.

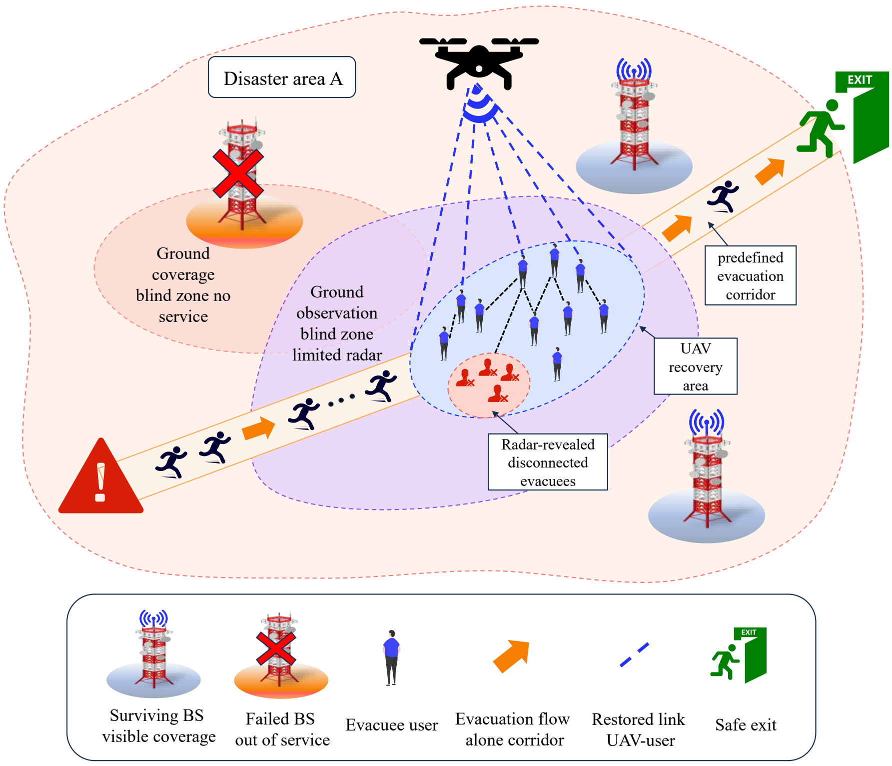

Figure 1. System scenario of UAV-BS aerial network recovery in a predefined evacuation corridor.

The horizontal location of each surviving ground base station $b \in \mathcal{B}_g$ is denoted by $\mathbf{q}_b \in \mathcal{A}$. The surviving network shows spatially non-uniform degradation after the disaster, including reduced coverage capability and limited demand visibility. These two types of degradation are modeled later through the ground coverage state and the network observation state.

A predefined evacuation corridor exists in the disaster area. It is determined by emergency plans, road-network conditions, or on-site command information and is denoted by

$$\mathcal{C}_e = \{\mathbf{c}(s) : s \in [0, L_e]\}, \tag{1}$$

where $\mathbf{c}(s) \in \mathcal{A}$ denotes the position along the corridor with arc-length parameter s, and L_e is the corridor length. This corridor connects hazardous areas, temporary gathering points, and safe exits. It represents the main spatial route along which evacuees move from dangerous areas to safe areas. The corridor is treated as fixed within each emergency decision period, while the UAV-BS recovery position can be updated across decision periods. If road conditions or on-site command decisions change, the corridor prior and the corresponding demand maps can be updated in the next decision period. To restore emergency communication service near the predefined evacuation corridor, the system deploys a UAV with both communication and sensing capabilities. The UAV operates at a fixed altitude H and serves as an aerial access node. During each emergency decision period, it is assumed to have access to at least one available emergency backhaul option with sufficient capacity for the considered recovery service. Such a backhaul option may be provided by a surviving base station with valid backhaul, an emergency command vehicle, a satellite link, or a temporary relay node. This condition represents the minimum operational requirement for real-time UAV-BS communication service. This paper focuses on access-side recovery position selection once a minimum emergency backhaul path is available rather than on how to construct the backhaul path itself. In the k-th emergency decision period, the horizontal location of the UAV is denoted by $\mathbf{p}(t_k) = [x(t_k), y(t_k)]^T \in \mathcal{A}$.

Different from coverage enhancement models that rely only on known user distributions, the UAV-BS considered here provides both aerial communication service and external sensing input. Therefore, the UAV location $\mathbf{p}(t_k)$ affects both its aerial service capability and the sensed evacuation state.

3.2. Sensing-Assisted Evacuee State Modeling

To characterize evacuation demand beyond network-side observations, the UAV-side sensing module provides external estimates of evacuee states near the predefined evacuation corridor. In this study, the sensing-state estimate is treated as the processed output of a UAV-mounted millimeter-wave FMCW radar module. The radar front end provides range–angle–Doppler detections, which are further converted into position, motion-state, and reliability estimates after ego-motion compensation, georeferencing, clustering, and tracking. The resulting noisy evacuee-state estimates are used as external inputs for communication recovery decisions. In the k-th emergency decision period, when the UAV is located at $\mathbf{p}(t_k)$, this radar-based sensing-state estimate is represented as

$$\mathcal{Z}(t_k) = \{(\mathbf{z}_i(t_k), \mathbf{v}_i(t_k), \omega_i(t_k))\}_{i=1}^{N_r(t_k)}, \tag{2}$$

where $\mathbf{z}_i(t_k)$, $\mathbf{v}_i(t_k)$, and $\omega_i(t_k)$ denote the position estimate, velocity estimate, and effective weight of the i-th evacuee target or crowd cluster, respectively. $N_r(t_k)$ denotes the number of effective sensed targets. Thus, $\mathcal{Z}(t_k)$ is treated as an abstract estimate of evacuee states. To describe sensing uncertainty, the position and velocity estimates are written as

$$\mathbf{z}_i(t_k) = \mathbf{u}_i(t_k) + \boldsymbol{\epsilon}_i^z(t_k), \tag{3}$$

$$\mathbf{v}_i(t_k) = \dot{\mathbf{u}}_i(t_k) + \boldsymbol{\epsilon}_i^v(t_k), \tag{4}$$

where $\mathbf{u}_i(t_k)$ and $\dot{\mathbf{u}}_i(t_k)$ denote the true position and velocity, respectively. The sensing error terms are modeled as

$$\boldsymbol{\epsilon}_i^z(t_k) \sim \mathcal{N}(\mathbf{0}, \sigma_s^2 \mathbf{I}_2), \quad \boldsymbol{\epsilon}_i^v(t_k) \sim \mathcal{N}(\mathbf{0}, \sigma_v^2 \mathbf{I}_2), \tag{5}$$

where σ_s and σ_v denote the position-estimation uncertainty and motion-estimation uncertainty, respectively.

The proposed model follows a discrete-time update structure. At each decision epoch t_k, the sensed evacuee states are used to reconstruct the density and flow fields for UAV-BS recovery position selection. If the sensing-to-decision delay is non-negligible, the sensed position can be propagated by a short-term motion model as

$$\hat{\mathbf{z}}_i(t_k + \tau_d) = \Pi_{\mathcal{A}}[\mathbf{z}_i(t_k) + \mathbf{v}_i(t_k)\tau_d], \tag{6}$$

where τ_d is the sensing-to-decision delay, and $\Pi_{\mathcal{A}}[\cdot]$ denotes projection onto the disaster area. The numerical evaluation adopts this short-lag setting with $\tau_d = 0$.

Based on $\mathcal{Z}(t_k)$, the sensing-revealed evacuee density field $\rho_r(\mathbf{u}, t_k)$ is defined as

$$\rho_r(\mathbf{u}, t_k) = \sum_{i=1}^{N_r(t_k)} \omega_i(t_k) K_\sigma(\mathbf{u} - \mathbf{z}_i(t_k)), \quad \mathbf{u} \in \mathcal{A}, \tag{7}$$

where $K_\sigma(\cdot)$ is specified as an isotropic Gaussian kernel,

$$K_\sigma(\mathbf{u} - \mathbf{z}_i(t_k)) = \frac{1}{2\pi\sigma^2} \exp\left(-\frac{\|\mathbf{u} - \mathbf{z}_i(t_k)\|^2}{2\sigma^2} \right). \tag{8}$$

where, σ denotes the KDE smoothing scale used to convert discrete sensing outputs into a continuous evacuee density field. It is different from the localization uncertainty σ_s in the sensing-error model: σ_s characterizes the random error in the sensed position estimate, whereas σ controls the spatial spread of each sensed target or crowd cluster in the density construction. In the simulations, the effective smoothing scale is set as

$$\sigma = \sqrt{\sigma_0^2 + \sigma_s^2}, \tag{9}$$

where σ_0 is the nominal KDE bandwidth. This setting makes the sensing-revealed density field smoother when the sensing-output localization uncertainty increases. This density field represents the spatial concentration of evacuees obtained from external sensing rather than the traffic density observed on the network side. The evacuation flow field is further defined as

$$\mathbf{f}_r(\mathbf{u}, t_k) = \frac{\sum_{i=1}^{N_r(t_k)} \omega_i(t_k) K_\sigma(\mathbf{u} - \mathbf{z}_i(t_k)) \mathbf{v}_i(t_k)}{\rho_r(\mathbf{u}, t_k) + \varepsilon}, \quad \mathbf{u} \in \mathcal{A}, \tag{10}$$

where $\varepsilon > 0$ is a regularization constant. $\mathbf{f}_r(\mathbf{u}, t_k)$ represents the dominant motion trend of local evacuees. Thus, $\rho_r(\mathbf{u}, t_k)$ and $\mathbf{f}_r(\mathbf{u}, t_k)$ form the sensing-state input for the subsequent demand map modeling.

3.3. Ground Coverage State and Network Observation State

The surviving ground base stations $\mathcal{B}_g$ form spatially non-uniform coverage in the area $\mathcal{A}$. For any location $\mathbf{u} \in \mathcal{A}$, we use the maximum signal-to-interference-plus-noise ratio (SINR) from the surviving base stations to describe the ground coverage state. Let $P_b(\mathbf{u}, t_k)$ denote the received power at location $\mathbf{u}$ from surviving base station $b \in \mathcal{B}_g$, which is given by

$$P_b(\mathbf{u}, t_k) = \frac{P_g}{(d_b(\mathbf{u}) + d_0)^{\eta_g}} \Theta(\mathbf{u}, t_k), \tag{11}$$

where P_g is the transmit power of a ground base station, $d_b(\mathbf{u}) = \|\mathbf{u} - \mathbf{q}_b\|$ is the horizontal distance from location $\mathbf{u}$ to base station b, d_0 is the reference distance, and η_g is the path-loss exponent of the ground link. $\Theta(\mathbf{u}, t_k)$ denotes a composite modulation term that captures disaster shadowing, local blockage, and other large-scale attenuation effects.

More specifically, the composite modulation term is introduced as a scenario-level large-scale coverage modulation field rather than a small-scale fading coefficient or a site-specific disaster propagation channel. Its purpose is to generate spatially non-uniform post-disaster coverage conditions caused by damaged sites, local blockage, and residual coverage variations by modulating the received power from the surviving ground base stations. It is constructed as a bounded and spatially correlated field,

$$\Theta(\mathbf{u}, t_k) = \mathrm{clip}\{\exp[-\zeta(\mathbf{u}, t_k)], \Theta_{\min}, \Theta_{\max}\}, \tag{12}$$

where $\Theta_{\min}$ and $\Theta_{\max}$ denote the lower and upper bounds of the modulation field, and the non-negative attenuation field $\zeta(\mathbf{u}, t_k)$ is generated by Gaussian spatial kernels,

$$\zeta(\mathbf{u}, t_k) = \kappa_{\mathrm{sh}} \sum_{m \in \mathcal{M}_s} a_m \exp\left(-\frac{\|\mathbf{u} - \mathbf{c}_m\|^2}{2s_m^2}\right) + \kappa_{\mathrm{bl}}\, g_e(\mathbf{u}). \tag{13}$$

where, $\mathcal{M}_s$ denotes the set of damaged or shadowed regions, and $\mathbf{c}_m$, a_m, and s_m are the center, weight, and spatial scale of the m-th region, respectively; $g_e(\mathbf{u})$ represents additional local blockage around the damaged corridor segment; and κ_{sh} and κ_{bl} control the strengths of large-scale shadowing and local blockage. The statistical assumption is that $\Theta(\mathbf{u}, t_k)$ is a smooth, bounded, and spatially correlated large-scale random field: across different post-disaster realizations, the centers and weights of the damaged regions are randomly perturbed, while the same large-scale statistical structure is retained so that $\Theta(\mathbf{u}, t_k)$ reflects environment-dependent large-scale coverage modulation rather than independent per-location fluctuation. Consequently, obstructed or shadowed regions affect the coverage state through reduced received power and SINR.

Based on the surviving base station set $\mathcal{B}_g$, the maximum SINR at location $\mathbf{u}$ is defined as

$$\gamma_g(\mathbf{u}, t_k) = \max_{b \in \mathcal{B}_g} \frac{P_b(\mathbf{u}, t_k)}{\sum_{j \in \mathcal{B}_g, j \neq b} P_j(\mathbf{u}, t_k) + N_0}, \tag{14}$$

where N_0 is the noise power. To capture the smooth transition from weak to strong coverage, $\gamma_g(\mathbf{u}, t_k)$ is converted into the dB scale as

$$\gamma_g^{\mathrm{dB}}(\mathbf{u}, t_k) = 10 \log_{10}\big(\gamma_g(\mathbf{u}, t_k) + \varepsilon_\gamma\big), \tag{15}$$

where ε_γ is a small positive constant used to avoid numerical singularity. The ground coverage state is then defined as

$$C_g(\mathbf{u}, t_k) = \frac{1}{1 + \exp\left[-a_c\left(\gamma_g^{\mathrm{dB}}(\mathbf{u}, t_k) - \gamma_{\mathrm{th}}^{\mathrm{dB}}\right)\right]}, \tag{16}$$

where $\gamma_{\mathrm{th}}^{\mathrm{dB}}$ is the coverage determination threshold, and a_c controls the sharpness of the soft transition from marginal to reliable coverage; in practice, it can be calibrated from the SINR transition width over which measured service reliability increases from weak to stable service. The threshold $\gamma_{\mathrm{th}}^{\mathrm{dB}}$ represents the SINR requirement associated with a minimum ground-link spectral efficiency $R_{\min}^{g}$, i.e.,

$$\gamma_{\mathrm{th}}^{\mathrm{dB}} = 10 \log_{10}\left(2^{R_{\min}^{g}} - 1\right). \tag{17}$$

where $R_{\min}^{g}$ denotes the minimum ground-link spectral efficiency requirement. $C_g(\mathbf{u}, t_k) \in [0, 1]$ represents the degree to which location $\mathbf{u}$ can obtain reliable communication service from the surviving ground base stations $\mathcal{B}_g$. The corresponding coverage blind-zone factor is defined as

$$B_c(\mathbf{u}, t_k) = 1 - C_g(\mathbf{u}, t_k). \tag{18}$$

The coverage state only describes the ground service capability. To describe the visibility of user states and communication demands on the network side, we introduce an observation visibility factor $\chi_g(\mathbf{u}, t_k) \in [0, 1]$. This factor captures the impact of access failures, silent terminals, limited status reporting, and backhaul blockage on network observation capability. The network observation state is further defined as

$$O_g(\mathbf{u}, t_k) = C_g(\mathbf{u}, t_k)\chi_g(\mathbf{u}, t_k). \tag{19}$$

The corresponding observation blind-zone factor is defined as

$$B_o(\mathbf{u}, t_k) = 1 - O_g(\mathbf{u}, t_k). \tag{20}$$

Thus, $O_g(\mathbf{u}, t_k)$ represents the overall network-side observability, which depends on both ground service availability and conditional demand visibility. Accordingly, $B_c(\mathbf{u}, t_k)$ represents ground service degradation, while $B_o(\mathbf{u}, t_k)$ represents network observation degradation. They serve as network-side state variables for the subsequent construction of the invisible-demand map.

3.4. Predefined Evacuation Corridor Relevance Modeling

To incorporate the predefined evacuation corridor into the subsequent demand map construction, we characterize the relationship between location $\mathbf{u}$ and $\mathcal{C}_e$ through corridor proximity and flow alignment. Corridor proximity is used to weight corridor-related demand intensity, while flow alignment describes the directional continuity of evacuation movement. The shortest distance from location $\mathbf{u} \in \mathcal{A}$ to the predefined evacuation corridor $\mathcal{C}_e$ is defined as

$$d_e(\mathbf{u}) = \min_{s\in[0,L_e]} \|\mathbf{u} - \mathbf{c}(s)\|. \tag{21}$$

The corridor proximity weight is then defined as

$$\psi_e(\mathbf{u}) = \exp\left(-\frac{d_e^2(\mathbf{u})}{2\sigma_e^2}\right), \tag{22}$$

where σ_e controls the spatial influence range of the predefined evacuation corridor. $\psi_e(\mathbf{u}) \in (0, 1]$ represents the spatial relevance between location $\mathbf{u}$ and the corridor.

Furthermore, let $s^\star(\mathbf{u})$ denote the nearest projection parameter of location $\mathbf{u}$ on the corridor:

$$s^\star(\mathbf{u}) = \arg\min_{s\in[0,L_e]} \|\mathbf{u} - \mathbf{c}(s)\|. \tag{23}$$

The corresponding local corridor direction is defined as

$$\mathbf{e}(\mathbf{u}) = \frac{\dot{\mathbf{c}}(s^\star(\mathbf{u}))}{\|\dot{\mathbf{c}}(s^\star(\mathbf{u}))\| + \varepsilon}, \tag{24}$$

where $\dot{\mathbf{c}}(s)$ is the tangent direction of the corridor curve, and $\varepsilon > 0$ is a regularization constant. Based on the sensed evacuation flow field $\mathbf{f}_r(\mathbf{u}, t_k)$, the flow-alignment factor is defined as

$$\alpha_e(\mathbf{u}, t_k) = \max\left\{0, \frac{\mathbf{f}_r^T(\mathbf{u}, t_k)\mathbf{e}(\mathbf{u})}{\|\mathbf{f}_r(\mathbf{u}, t_k)\|\|\mathbf{e}(\mathbf{u})\| + \varepsilon}\right\}. \tag{25}$$

where, $\alpha_e(\mathbf{u}, t_k) \in [0, 1]$ represents the alignment between the local evacuation flow and the corridor direction. This rectified cosine form is consistent with desired-direction modeling in pedestrian dynamics and velocity-coherence measures in crowd analysis [33,34]. For invisible-demand construction, the corridor relevance weight is defined as

$$\omega_e(\mathbf{u}) = 1 + \lambda_c\psi_e(\mathbf{u}), \tag{26}$$

where $\lambda_c \geq 0$ controls how corridor proximity enhances the communication demand weight. The constant term in $\omega_e(\mathbf{u})$ preserves off-corridor invisible demand, while $\psi_e(\mathbf{u})$ enhances demand near the predefined evacuation corridor. The weight $\omega_e(\mathbf{u})$ is used in the subsequent construction of the invisible-demand map, while the flow-alignment factor $\alpha_e(\mathbf{u}, t_k)$ is used to construct the evacuation-flow demand map.

4. Aerial Network Recovery Problem

4.1. Effective Blind-Zone Factor and Demand Map Generation

The emergency communication demand near the predefined evacuation corridor depends on the evacuee state obtained from sensing outputs, the degraded ground network state, and corridor relevance. To form the spatial demand input for UAV-BS recovery position selection, the evacuee density $\rho_r(\mathbf{u}, t_k)$, the effective blind-zone factor, and the corridor relevance weight $\omega_e(\mathbf{u})$ are mapped into an invisible-demand map. This map characterizes communication demand near the predefined corridor that is inferred from sensing outputs but cannot be reliably served or observed by the surviving ground network.

The effective blind-zone factor describes both service degradation and observation degradation on the ground-network side. Specifically, $C_g(\mathbf{u}, t_k)$ describes the service capability of the surviving ground network at location $\mathbf{u}$, while $\chi_g(\mathbf{u}, t_k)$ describes the visibility of user states and communication demands on the network side. Based on these two terms, the effective blind-zone factor is defined as

$$B_{\text{eff}}(\mathbf{u}, t_k) = 1 - C_g(\mathbf{u}, t_k)\left[\chi_g(\mathbf{u}, t_k)\right]^{\beta_o}, \tag{27}$$

where $\beta_o \geq 0$ is the observation-degradation control parameter. A larger $B_{\text{eff}}(\mathbf{u}, t_k)$ indicates stronger ground service degradation or demand visibility degradation at location $\mathbf{u}$. This definition retains the distinction between service availability and demand visibility: C_g describes whether a location can be served, whereas χ_g describes whether demand at that location can be observed. The parameter β_o adjusts the relative impact of observation degradation in the recovery demand map.

By combining the evacuee density field obtained from sensing outputs, $\rho_r(\mathbf{u}, t_k)$, the effective blind-zone factor $B_{\text{eff}}(\mathbf{u}, t_k)$, and the corridor relevance weight $\omega_e(\mathbf{u})$, the invisible-demand map is defined as

$$D_{\text{inv}}(\mathbf{u}, t_k) = \rho_r(\mathbf{u}, t_k)[B_{\text{eff}}(\mathbf{u}, t_k)]^{\alpha_b}\omega_e(\mathbf{u}), \quad \mathbf{u} \in \mathcal{A}, \tag{28}$$

where $\alpha_b \geq 0$ controls the impact of the effective blind-zone factor on the invisible-demand intensity. This definition assigns larger values to locations with sensed evacuee presence, stronger ground-network degradation, and higher corridor relevance. Thus, D_{inv} characterizes evacuation communication demand that the network side cannot reliably serve or observe.

In addition to invisible-demand intensity, crowd movement in the predefined evacuation corridor also has directionality and continuity. To characterize the movement intensity of the local evacuation flow, the normalized evacuation speed factor is defined as

$$\bar{v}_r(\mathbf{u}, t_k) = \frac{\|\mathbf{f}_r(\mathbf{u}, t_k)\|}{v_{\max} + \varepsilon}, \tag{29}$$

where $v_{\max}$ is the reference maximum evacuation speed and $\varepsilon > 0$ is a regularization constant. Based on the evacuee density field $\rho_r(\mathbf{u}, t_k)$, the corridor proximity weight $\psi_e(\mathbf{u})$, the flow-alignment factor $\alpha_e(\mathbf{u}, t_k)$, and the normalized evacuation speed factor $\bar{v}_r(\mathbf{u}, t_k)$, the evacuation-flow demand map is defined as

$$D_{\text{flow}}(\mathbf{u}, t_k) = \rho_r(\mathbf{u}, t_k)\psi_e(\mathbf{u})\alpha_e(\mathbf{u}, t_k)\bar{v}_r(\mathbf{u}, t_k), \quad \mathbf{u} \in \mathcal{A}. \tag{30}$$

While $D_{\text{inv}}(\mathbf{u}, t_k)$ characterizes invisible communication demand, $D_{\text{flow}}(\mathbf{u}, t_k)$ focuses on the continuous communication demand of evacuation flows along the predefined corridor. This map is jointly modulated by corridor proximity, flow alignment, and movement intensity. Together with $D_{\text{inv}}(\mathbf{u}, t_k)$, it serves as the demand input for the subsequent UAV-BS recovery criterion.

4.2. UAV-BS Recovery Criterion Based on Demand Maps

To convert the above demand maps into a UAV-BS position selection criterion, the composite demand function is first defined as

$$W(\mathbf{u}, t_k) = D_{\text{inv}}(\mathbf{u}, t_k) + \mu D_{\text{flow}}(\mathbf{u}, t_k), \tag{31}$$

where $\mu \geq 0$ is the evacuation-flow demand weight that adjusts the contribution of continuous communication demand in the recovery criterion. $W(\mathbf{u}, t_k)$ represents the composite recovery demand intensity at location $\mathbf{u}$ in the k-th decision period.

Let $\mathbf{p}_h \in \mathcal{A}$ denote the candidate recovery position selected by the UAV in the k-th emergency decision period, and let $\mathbf{p}(t_k)$ denote its current position. For any ground location $\mathbf{u} \in \mathcal{A}$, the air-to-ground distance is

$$d_a(\mathbf{p}_h, \mathbf{u}) = \sqrt{H^2 + \|\mathbf{p}_h - \mathbf{u}\|^2}, \tag{32}$$

where H is the UAV flight altitude. To keep the focus on recovery decisions rather than physical-layer channel optimization, the air-to-ground link is modeled by an equivalent distance-dependent SNR:

$$\gamma_a(\mathbf{p}_h, \mathbf{u}) = \frac{\Gamma_a}{d_a^2(\mathbf{p}_h, \mathbf{u})} = \frac{\Gamma_a}{H^2 + \|\mathbf{p}_h - \mathbf{u}\|^2}, \tag{33}$$

where Γ_a is an equivalent air-to-ground gain that absorbs the UAV-BS transmit power, reference channel gain, and noise power. Considering that a fraction ξ of the time is used for sensing, the effective air-to-ground link rate is given by

$$R_a(\mathbf{p}_h, \mathbf{u}) = (1 - \xi)\log_2(1 + \gamma_a(\mathbf{p}_h, \mathbf{u})), \tag{34}$$

where $\xi \in [0, 1)$ is the sensing time fraction and $(1 - \xi)$ denotes the time fraction used for communication service.

To avoid reducing aerial service capability to a binary coverage decision, the smooth aerial service probability is defined as

$$S_a(\mathbf{p}_h, \mathbf{u}) = \frac{1}{1 + \exp[-\kappa_s(R_a(\mathbf{p}_h, \mathbf{u}) - R_{\min})]}, \tag{35}$$

where $R_{\min}$ is the minimum service-rate threshold, and κ_s is the smooth-threshold coefficient that controls the slope of the transition from low to high service probability around $R_a(\mathbf{p}_h, \mathbf{u}) = R_{\min}$. $S_a(\mathbf{p}_h, \mathbf{u}) \in [0, 1]$ represents the degree to which location $\mathbf{u}$ can obtain effective aerial communication service when the UAV is located at $\mathbf{p}_h$.

Based on the composite demand function and the aerial service probability, the demand-weighted recovery utility of the UAV at candidate position $\mathbf{p}_h$ is defined as

$$\begin{aligned} J(\mathbf{p}_h, t_k) &= \int_{\mathcal{A}} W(\mathbf{u}, t_k) S_a(\mathbf{p}_h, \mathbf{u})\, \mathrm{d}\mathbf{u} - \eta_m \|\mathbf{p}_h - \mathbf{p}(t_k)\|^2 \\ &= \int_{\mathcal{A}} [D_{\text{inv}}(\mathbf{u}, t_k) + \mu D_{\text{flow}}(\mathbf{u}, t_k)] S_a(\mathbf{p}_h, \mathbf{u})\, \mathrm{d}\mathbf{u} - \eta_m \|\mathbf{p}_h - \mathbf{p}(t_k)\|^2. \end{aligned} \tag{36}$$

where, $\eta_m \geq 0$ is the UAV maneuvering-cost coefficient. The integral term represents the matching gain between the UAV aerial service capability and the composite demand distribution, while the second term represents the response cost caused by moving the UAV from its current position $\mathbf{p}(t_k)$ to the candidate recovery position $\mathbf{p}_h$.

Let $V_{\max}$ denote the maximum UAV flight speed and T_r denote the available response time within one decision period. The response radius is then given by $R_r = V_{\max} T_r$. The feasible candidate-position set in the k-th emergency decision period is defined as

$$\mathcal{P}(t_k) = \{\mathbf{p}_h \in \mathcal{A} : \|\mathbf{p}_h - \mathbf{p}(t_k)\| \leq R_r\}. \tag{37}$$

Thus, the UAV-BS recovery position selection problem based on demand maps is formulated as

$$\mathbf{P1}: \quad \max_{\mathbf{p}_h} \quad \int_{\mathcal{A}} [D_{\text{inv}}(\mathbf{u}, t_k) + \mu D_{\text{flow}}(\mathbf{u}, t_k)] S_a(\mathbf{p}_h, \mathbf{u})\, \mathrm{d}\mathbf{u} - \eta_m \|\mathbf{p}_h - \mathbf{p}(t_k)\|^2 \tag{38a}$$

$$\text{s.t.} \quad \mathbf{p}_h \in \mathcal{P}(t_k). \tag{38b}$$

where, $\mathcal{P}(t_k)$ denotes the reachable horizontal candidate-position set constrained by the disaster-area boundary and the response radius in the current decision period.

The current formulation focuses on single-period UAV-BS recovery position selection. The response radius R_r limits the reachable region within one decision period, and the maneuvering-cost term penalizes long-distance relocation. These terms provide a simplified mobility-related constraint, but they do not replace a hard UAV energy-budget constraint. An energy-aware extension can further restrict the feasible set by considering flight, hovering, communication, and sensing energy consumption, e.g.,

$$E_{\text{fly}}(\mathbf{p}_h, t_k) + E_{\text{hov}}(t_k) + E_{\text{comm}}(t_k) + E_{\text{sens}}(t_k) \leq E_{\text{ava}}(t_k), \tag{39}$$

where $E_{\text{ava}}(t_k)$ denotes the available onboard energy in the current decision period. Incorporating this constraint leads to an energy-aware multi-period UAV-BS recovery problem, which is left for future work.

4.3. Adaptive Position Search Algorithm Guided by Demand Maps

Problem **P1** is determined by the composite demand function, the aerial service probability, and the UAV maneuvering cost. It is generally difficult to obtain a closed-form optimal solution. A global dense grid search can find the optimal position over a discrete candidate set, but it also produces many unnecessary evaluations in low-demand areas. To support fast response in post-disaster emergency scenarios, we adopt a lightweight adaptive position search algorithm guided by the constructed demand maps to solve **P1**. The algorithm uses the composite demand function $W(\mathbf{u}, t_k)$ to guide candidate-region generation and the recovery utility function $J(\mathbf{p}_h, t_k)$ to retain candidates with high recovery utility.

First, the disaster area $\mathcal{A}$ is discretized into a ground evaluation grid

$$\mathcal{G} = \{\mathbf{u}_g\}_{g=1}^{G}, \tag{40}$$

where G is the number of grid points. For discrete search, the continuous feasible set $\mathcal{P}(t_k)$ is discretized on the grid $\mathcal{G}$, which gives the initial reachable candidate set

$$\mathcal{P}_c^{(0)}(t_k) = \mathcal{P}(t_k) \cap \mathcal{G} = \{\mathbf{p}_n \in \mathcal{G} : \|\mathbf{p}_n - \mathbf{p}(t_k)\| \leq R_r\}, \tag{41}$$

where $\mathbf{p}_n$ denotes the n-th discrete candidate position. This set represents the reachable horizontal positions of the UAV in the current decision period.

Based on the composite demand function $W(\mathbf{u}, t_k)$, the algorithm selects K spatially separated high-demand positions from $\mathcal{P}_c^{(0)}(t_k)$ as initial candidate positions. To prevent these positions from being concentrated around the same local demand peak, a minimum-distance constraint d_{sep} is imposed during selection. Let $\mathcal{Q}_c(t_k)$ denote the initial candidate-position set. Then,

$$\mathcal{Q}_c(t_k) \subseteq \mathcal{P}_c^{(0)}(t_k), \quad |\mathcal{Q}_c(t_k)| = K, \tag{42}$$

and any two different initial candidate positions satisfy

$$\|\mathbf{q}_i - \mathbf{q}_j\| \geq d_{\mathrm{sep}}, \quad \forall \mathbf{q}_i, \mathbf{q}_j \in \mathcal{Q}_c(t_k),\ i \neq j. \tag{43}$$

The initial candidate positions are selected in descending order of $W(\mathbf{u}, t_k)$ and used to initialize local search centers.

To reduce the dependence of the selection of the K highest-demand positions on local peaks, the algorithm further introduces a demand-centroid candidate position. In the reachable candidate set, grid points whose $W(\mathbf{u}_g, t_k)$ values are higher than the q_c-th percentile threshold are selected to form the high-demand subset

$$\mathcal{G}_c(t_k) = \left\{ \mathbf{u}_g \in \mathcal{P}_c^{(0)}(t_k) : W(\mathbf{u}_g, t_k) \geq Q_{q_c} \right\}, \tag{44}$$

where Q_{q_c} is the q_c-th percentile threshold of W over $\mathcal{P}_c^{(0)}(t_k)$. The corresponding demand-centroid candidate position is defined as

$$\mathbf{q}_c(t_k) = \frac{\sum_{\mathbf{u}_g \in \mathcal{G}_c(t_k)} W(\mathbf{u}_g, t_k)\mathbf{u}_g}{\sum_{\mathbf{u}_g \in \mathcal{G}_c(t_k)} W(\mathbf{u}_g, t_k) + \varepsilon}, \tag{45}$$

where $\varepsilon > 0$ is a regularization constant. This demand-centroid candidate position provides an additional search entry for compromise positions among multiple high-demand regions.

After candidate-position initialization, the algorithm uses the discrete recovery utility to screen candidate positions. For any candidate position $\mathbf{p}$, the discrete form of the continuous recovery utility $J(\mathbf{p}, t_k)$ is given by

$$J_d(\mathbf{p}, t_k) = \sum_{g=1}^{G} W(\mathbf{u}_g, t_k) S_a(\mathbf{p}, \mathbf{u}_g) \Delta A - \eta_m \|\mathbf{p} - \mathbf{p}(t_k)\|^2, \tag{46}$$

where ΔA is the area of a grid cell. The algorithm keeps the K_s positions with the highest J_d values from the initial candidate-position set $\mathcal{Q}_c(t_k) \cup \{\mathbf{q}_c(t_k)\}$, forming the initial local-center set $\mathcal{C}^{(0)}(t_k)$.

The algorithm then performs multi-scale local refinement around the retained centers. Let the refinement radius sequence be

$$\mathcal{R} = \{r_1, r_2, \ldots, r_L\}, \quad r_1 > r_2 > \cdots > r_L > 0, \tag{47}$$

where L is the number of refinement rounds. In the ℓ-th refinement round, for each retained center $\mathbf{c} \in \mathcal{C}^{(\ell-1)}(t_k)$, the algorithm generates two-scale candidate points along N_θ sampled angular directions:

$$\mathcal{N}_\ell(\mathbf{c}) = \left\{ \mathbf{c} + \rho \begin{bmatrix} \cos\theta_m \\ \sin\theta_m \end{bmatrix} : \rho \in \left\{ r_\ell, \frac{r_\ell}{2} \right\}, m = 1, \ldots, N_\theta \right\} \cap \mathcal{P}(t_k), \tag{48}$$

where $\theta_m = 2\pi(m-1)/N_\theta$. The local candidate set in the ℓ-th round is

$$\mathcal{P}_c^{(\ell)}(t_k) = \bigcup_{\mathbf{c}\in\mathcal{C}^{(\ell-1)}(t_k)} \mathcal{N}_\ell(\mathbf{c}). \tag{49}$$

The algorithm selects the K_s positions with the highest J_d values from $\mathcal{P}_c^{(\ell)}(t_k)$ as the local search centers $\mathcal{C}^{(\ell)}(t_k)$ for the next round. As the refinement radius decreases round by round, the search process moves from rough localization to local fine adjustment.

After L refinement rounds, let $\mathcal{P}_{\text{ref}}(t_k)$ denote the set of all evaluated candidate positions. The final UAV-BS recovery position is obtained by selecting the candidate with the largest evaluated discrete recovery utility:

$$\mathbf{p}_h^\star(t_k) = \arg\max_{\mathbf{p}\in\mathcal{P}_{\text{ref}}(t_k)} J_d(\mathbf{p}, t_k). \tag{50}$$

Since all evaluated candidate positions are stored in $\mathcal{P}_{\text{ref}}(t_k)$, the maximum evaluated value of $J_d(\mathbf{p}, t_k)$ over this set does not decrease as more candidates are added. Because the reachable candidate set is finite and $J_d(\mathbf{p}, t_k)$ is bounded on this set, the search reaches a stable discrete solution after the predefined number of refinement rounds.

The discretization scale also affects the approximation accuracy. If the continuous recovery utility is Lipschitz continuous on the compact feasible region with constant L_J, and if $\mathbf{p}^\star$ and $\mathbf{p}_\Delta^\star$ denote the continuous-space optimum and the full-grid optimum, respectively, then the discretization-induced gap satisfies

$$0 \le J(\mathbf{p}^\star, t_k) - J(\mathbf{p}_\Delta^\star, t_k) \le L_J \delta_g, \tag{51}$$

where δ_g is the covering radius of the discretized candidate grid. For a square grid with spacing Δ_g, the covering radius satisfies $\delta_g \le \sqrt{2}\Delta_g/2$. Thus, a finer grid reduces the discretization-induced approximation gap, but it also increases the number of recovery-utility evaluations.

The refinement radius sequence controls the balance between coarse exploration and local exploitation. The first radius determines the exploration range around high-demand initial candidates, while the later radii progressively refine the selected position. In practice, the final radius is chosen to be comparable to the grid scale. Further refinement below this scale provides limited performance improvement because the effective search resolution is already constrained by the evaluation grid. By combining candidate-position initialization based on demand maps, screening based on recovery utility, and local refinement with shrinking radii, the algorithm limits detailed evaluation to a small set of high-value candidate regions.

Algorithm 1 summarizes the main steps of the adaptive position search.

If a global dense grid search is used, let N_c denote the number of reachable candidate positions. The aerial service probability and demand-weighted utility need to be evaluated for all candidate positions, leading to a complexity of $\mathcal{O}(GN_c)$, where G is the number of ground evaluation grid points. In contrast, the proposed search first selects K spatially separated high-demand candidate positions and keeps K_s local centers after screening based on recovery utility. It then generates candidate points around each local center along N_θ directions over L refinement rounds. Therefore, the number of evaluated candidate positions is approximately $\mathcal{O}(K + LK_sN_\theta)$. Since each candidate position requires evaluating $S_a(\mathbf{p}, \mathbf{u}_g)$ and the corresponding demand-weighted utility over G ground grid points, the overall complexity of the search process is approximately $\mathcal{O}(G(K + LK_sN_\theta))$.

Because $K + LK_sN_\theta$ is usually much smaller than the number of globally reachable candidates N_c, the search method reduces the number of candidate-position evaluations, especially in low-demand regions.

Algorithm 1 Adaptive Position Search Algorithm Guided by Demand Maps

```
Input: Current UAV position p(t_k); evaluation grid G; feasible set P(t_k); composite
  demand function W(u, t_k); search parameters K, K_s, d_sep, q_c, R = {r_1, ..., r_L}, and N_θ.
Output: UAV-BS recovery position p_h^⋆(t_k).
Discretize P(t_k) on G to obtain the initial reachable candidate set
    P_c^(0)(t_k) = P(t_k) ∩ G.
Select K high-demand positions from P_c^(0)(t_k) according to W(u, t_k) under the
  minimum-distance constraint d_sep and form the initial candidate-position set Q_c(t_k).
Construct the high-demand subset using the q_c-th percentile threshold, and compute
  the demand-centroid candidate position q_c(t_k).
Construct the initial candidate set
    Q_0(t_k) = Q_c(t_k) ∪ {q_c(t_k)}.
Evaluate the discrete recovery utility J_d for each candidate position in Q_0(t_k), and keep
  the K_s positions with higher utility values as the initial local search-center set C^(0)(t_k).
Initialize the evaluated candidate set
    P_ref(t_k) ← Q_0(t_k).
for ℓ = 1 to L do
  Initialize P_c^(ℓ)(t_k) ← ∅.
  for each c ∈ C^(ℓ−1)(t_k) do
    Generate local candidate points along N_θ angular directions with radii r_ℓ and r_ℓ/2.
    Keep the candidates satisfying the constraint P(t_k) and add them to P_c^(ℓ)(t_k).
  end for
  Evaluate the discrete recovery utility J_d for each candidate position in P_c^(ℓ)(t_k).
  Update P_ref(t_k) ← P_ref(t_k) ∪ P_c^(ℓ)(t_k).
  Select the K_s positions with higher J_d values from P_c^(ℓ)(t_k) as the local search-center
    set C^(ℓ)(t_k) for the next round.
end for
Output
    p_h^⋆(t_k) = arg max_{p ∈ P_ref(t_k)} J_d(p, t_k).
return p_h^⋆(t_k).
```

5. Simulation Results

This section evaluates the proposed sensing-assisted UAV-BS aerial network recovery method for predefined evacuation corridors. The simulations illustrate the construction of demand maps, compare different UAV-BS deployment criteria, and examine the effects of response radius and sensing-output localization uncertainty.

The simulated disaster area is $\mathcal{A} = [-500, 500] \times [-500, 500]$ m^2 and is discretized into an 81×81 ground evaluation grid. A predefined evacuation corridor is represented by a disaster-map polyline from the hazardous area toward the safe-exit direction. Evacuee demand is heterogeneous: some demand can be observed by the surviving network, some is located near the corridor but is weakly visible to the network, and a small number of disconnected evacuees appear away from the corridor. This setting allows us to test whether each deployment criterion can respond to visible demand, invisible demand, and continuous communication demand along the evacuation flow.

The ground coverage state is generated using the max-SINR model in Section 3 and mapped through a smooth threshold function. The network observation state is modeled by a conditional visibility factor that captures limited access and status reporting. These two states form the effective blind-zone factor used in the invisible-demand map. The UAV operates at altitude $H = 110$ m with initial horizontal position $\mathbf{p}(t_0) = (-360, -330)$ m and response radius $R_r = 410$ m. The aerial service probability follows the smooth rate-threshold model in Section 4, with $\xi = 0.18$, $\Gamma_a = 7.0 \times 10^5$, $R_{\min} = 3.58$ bps/Hz, and $\kappa_s = 3.4$. The sensing output is modeled as noisy evacuee-state observations, with a default localization uncertainty of 8 m and a KDE bandwidth of 28 m.

The proposed method uses both the invisible-demand map and the evacuation-flow demand map for UAV-BS recovery position selection. The adaptive search algorithm selects $K = 10$ initial high-demand candidates, keeps $K_s = 4$ local centers after recovery-utility screening, and refines them with $N_\theta = 8$ angular directions and radii $\{170, 75, 30\}$ m. The main comparison is averaged over 12 randomized post-disaster realizations, and each sensitivity experiment uses 12 Monte Carlo runs for each parameter setting. The main simulation parameters are summarized in Table 2.

Table 2. Simulation parameters.

Parameter	Value
Post-disaster area $\mathcal{A}$	$1000 \text{ m} \times 1000$ m
Ground evaluation grid size	81×81
Number of surviving ground BSs	3
UAV altitude H	110 m
Initial UAV position $\mathbf{p}(t_0)$	$(-360, -330)$ m
Response radius R_r	410 m
Equivalent air-to-ground link gain Γ_a	7.0×10^5
Sensing time fraction ξ	0.18
Minimum service-rate threshold $R_{\min}$	3.58 bps/Hz
Smooth-threshold coefficient κ_s	3.4
UAV maneuvering-cost coefficient η_m	7.0×10^{-7}
Sensing KDE bandwidth	28 m
Disaster-shadowing coefficient κ_{sh}	3.0
Corridor-blockage coefficient κ_{bl}	1.2
Number of initial candidate positions K	10
Number of retained local search centers K_s	4
Number of angular samples N_θ	8
Refinement radius sequence $\mathcal{R}$	$\{170, 75, 30\}$ m
Minimum candidate-position separation d_{sep}	90 m
Demand-centroid percentile threshold q_c	94%
Monte Carlo runs for main comparison	12
Monte Carlo runs for sensitivity tests	12

Unless otherwise specified, the demand-map parameters are fixed as $\alpha_b = 0.95$, $\beta_o = 1.25$, $\lambda_c = 1.45$, and $\mu = 1.60$ throughout the simulations. These parameters are used to balance normalized demand-map components and are kept unchanged for all compared schemes.

5.1. Baselines and Performance Metrics

To fairly evaluate the impact of different spatial demand constructions on UAV-BS recovery decisions, all deployment schemes use the same UAV aerial service model, reachability constraint, and adaptive position search algorithm. The only difference lies in the spatial weight used for position selection. Therefore, the performance difference mainly reflects the effect of demand modeling on UAV-BS recovery position selection. Table 3 summarizes the compared deployment criteria.

Table 3. Compared deployment criteria.

Scheme	Position-Selection Weight
Cellular metric [14]	A position-selection weight based on network-side visible states from the surviving ground infrastructure.
Density only [26]	$\rho_r(\mathbf{u}, t_k)$, which selects the UAV-BS position only according to the sensed evacuee density.
Coverage-hole only [15]	$\rho_r(\mathbf{u}, t_k)B_c(\mathbf{u}, t_k)$, which prioritizes evacuee demand in coverage-degraded areas.
Blind-zone only	$\rho_r(\mathbf{u}, t_k)B_{\text{eff}}(\mathbf{u}, t_k)$, which considers ground service degradation and demand visibility degradation without explicitly modeling evacuation-flow continuity.
Proposed	$D_{\text{inv}}(\mathbf{u}, t_k) + \mu D_{\text{flow}}(\mathbf{u}, t_k)$, which jointly considers invisible-demand recovery and continuous communication demand along the evacuation flow.

To quantify recovery performance from different perspectives, we adopt the following metrics. These metrics are defined for the proposed blind-zone recovery scenario by referring to commonly used coverage, recovery, path-support, and edge-rate evaluation ideas in UAV-BS and evacuation-related studies. DCR and DRR measure the coverage of invisible demand and the recovery of disconnected regions, respectively. DW-EPC evaluates communication support along the predefined evacuation corridor, while $R_{5\%}$ reflects edge communication performance at weakly served locations.

- DCR: The demand coverage ratio, inspired by coverage-hole recovery evaluation in UAV-BS deployment [15], which measures the coverage of the invisible-demand map D_{inv} by the UAV aerial service.
- DRR: The disconnected-user recovery ratio, related to user recovery and mobile aerial base-station response studies [35], which measures the fraction of evacuees served by the UAV in coverage-degraded or observation-degraded regions.
- DW-EPC: The demand-weighted evacuation-path coverage, motivated by evacuation-corridor and crowd-evacuation modeling [3], which measures the communication support for evacuees near the predefined evacuation corridor.
- $R_{5\%}$: The edge evacuee rate, defined as the fifth percentile of the air-to-ground link rate over the evacuee region identified by aerial sensing. Similar percentile or edge-rate measures are commonly used to evaluate weak-user service quality in UAV-assisted emergency communications [9].

5.2. Simulation Results and Discussion

Following the system scenario in Figure 1, Figure 2 shows a representative UAV-BS recovery result. A predefined evacuation corridor connects the hazardous area and the safe exit, while the damaged ground network creates both coverage blind zones and observation blind zones along the evacuation process. These two blind-zone types are not equivalent: the former indicates degraded ground service capability, whereas the latter indicates limited network-side visibility of evacuee states and communication demands.

The UAV-BS provides temporary aerial recovery for evacuees near the predefined corridor. Its sensing function helps to reveal disconnected evacuees that may not be reliably observed by the surviving ground network, and its communication function provides restored UAV–user links in the local recovery area. This scenario motivates the subsequent construction of the invisible-demand map and the evacuation-flow demand map.

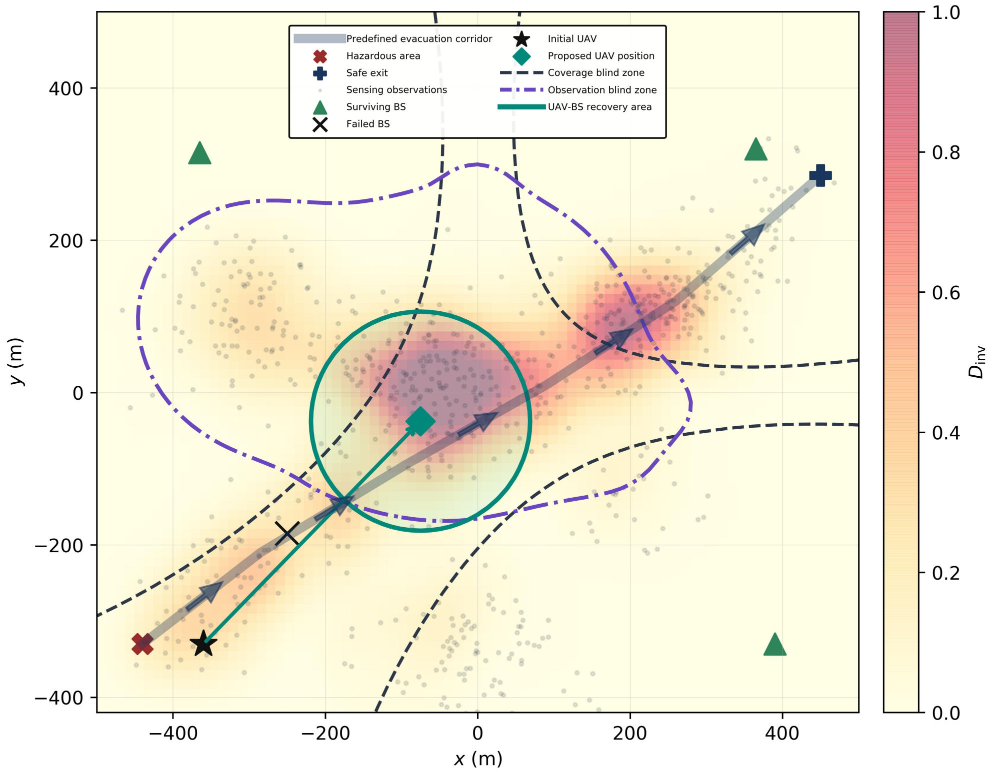

Figure 2. Representative UAV-BS recovery result in a predefined evacuation corridor.

Figure 3 further shows the construction of the invisible-demand map from its intermediate components. The sensing density ρ_r in Figure 3a reflects the spatial distribution of evacuees, while the coverage blindness $1 - C_g$ in Figure 3b reflects the degradation of ground service capability. These two maps are not fully consistent in space, indicating that high-density crowd regions do not necessarily correspond to high-priority regions for communication recovery. Figure 3c introduces the blindness–urgency factor, which combines the effective blind-zone state with relevance to the predefined evacuation corridor. This makes recovery-priority regions more concentrated in degraded areas near the corridor. Figure 3d shows that the final D_{inv} forms high-value areas where the sensed evacuee distribution, ground-network degradation, and corridor relevance are all strong. Compared with the original sensing density, D_{inv} weakens areas with lower relevance to recovery along the predefined corridor and highlights invisible communication demands near the corridor. This result demonstrates that the proposed demand map transforms sensing states and ground-network degradation states into spatial priorities that are more suitable for UAV-BS recovery position selection.

Figure 4 presents the performance comparison under different UAV-BS deployment criteria. The cellular metric baseline performs the worst, with DCR, DRR, and DW-EPC all below 0.1, showing that network-side visible information alone is insufficient for recovering invisible post-disaster demands. The DCR of density only increases to 0.317, indicating that sensing density can provide additional information about evacuee distribution, but it is still insufficient to determine whether these evacuees are located in priority recovery areas. Compared with density only, coverage-hole only improves DW-EPC and $R_{5\%}$, but its DCR and DRR decrease. This suggests that using coverage degradation as the deployment weight can improve service quality near coverage-degraded regions, but it does not fully capture invisible-demand recovery. Blind-zone only achieves the highest DRR, which is expected because it directly favors effective blind-zone regions. However, its DCR, DW-EPC, and composite score remain lower than those of the proposed scheme.

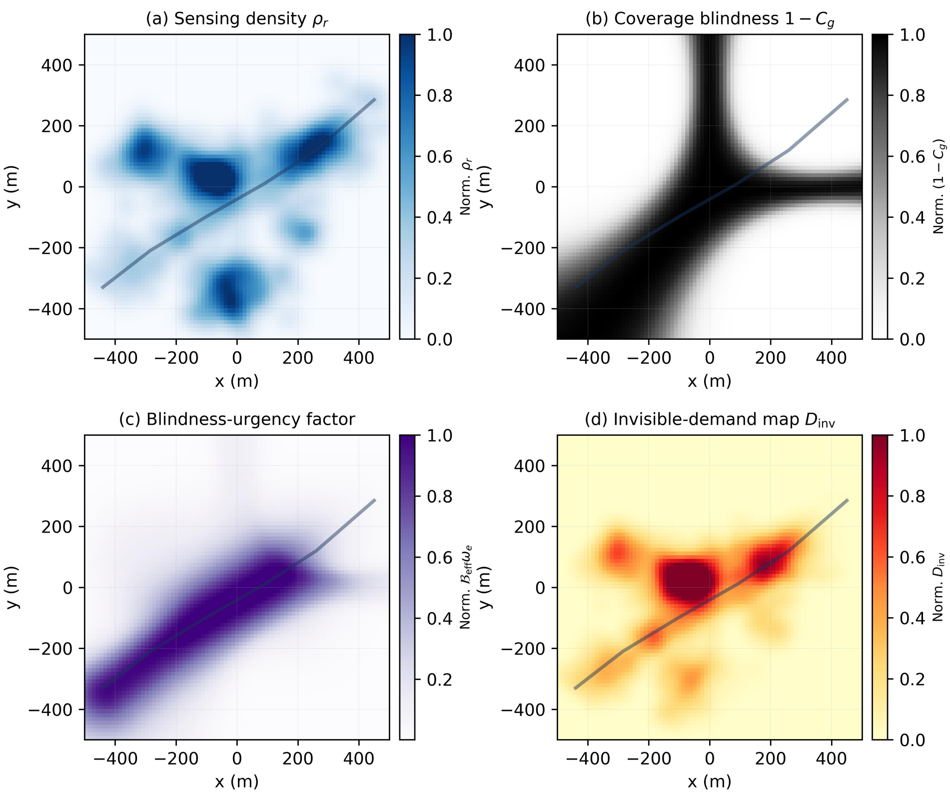

Figure 3. Construction of the invisible-demand map.

The proposed scheme achieves the highest DCR, DW-EPC, and $R_{5\%}$ while keeping DRR close to that of blind-zone only. Specifically, compared with the blind-zone-only baseline, the proposed scheme improves the DCR from 0.365 to 0.373, the DW-EPC from 0.286 to 0.316, and the edge evacuee rate $R_{5\%}$ from 1.559 to 1.672 bps/Hz. In Figure 4b, it also obtains the highest composite recovery score, reaching 0.481. This confirms that combining the invisible-demand map with the evacuation-flow demand map yields a more balanced recovery decision across invisible-demand coverage, disconnected-region recovery, corridor-continuity support, and edge-rate guarantee.

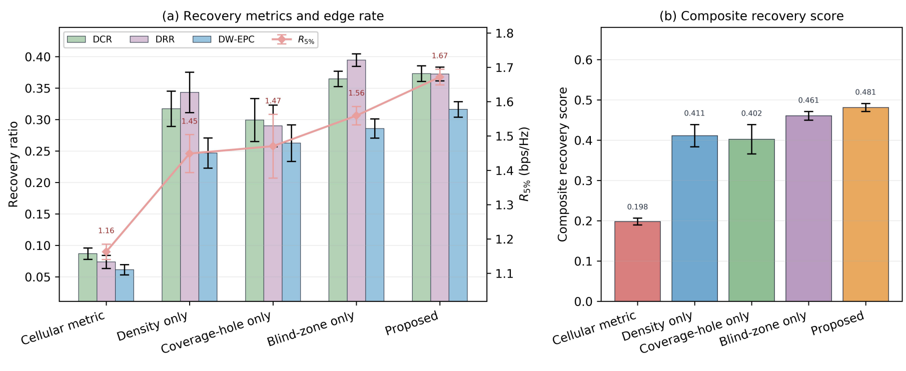

Figure 4. Recovery performance under different UAV-BS deployment criteria. (**a**) Recovery metrics and edge rate. (**b**) Composite recovery score.

Figure 5 shows the effect of the emergency response radius on DW-EPC. As R_r increases, most schemes obtain higher DW-EPC except for the cellular metric. This trend is reasonable because a larger reachable region allows the UAV-BS to move closer to high-demand areas near the predefined evacuation corridor. As a result, the evacuation-path coverage can be improved when the position-selection criterion is related to corridor demand.

The proposed scheme achieves the highest or near-highest DW-EPC under most response radii. Its advantage becomes clearer when $R_r \geq 260$ m. This indicates that, once the UAV-BS has enough mobility, jointly using D_{inv} and D_{flow} helps in selecting recovery positions that are closer to continuous corridor demand. In contrast, the cellular metric remains low and may even decrease as R_r increases. This is because it relies on network-visible states. When the reachable region becomes larger, it may select visible but corridor-irrelevant areas, which do not contribute much to DW-EPC.

Density only improves when the response radius becomes large, especially after $R_r = 340$ m. This suggests that density-based deployment needs sufficient mobility to approach the main sensed crowd region. However, it is less stable than the proposed scheme because it does not explicitly consider corridor continuity or network degradation. Coverage-hole only and blind-zone only also benefit from a larger response radius, but they remain below the proposed scheme at large radii. This shows that coverage degradation and blind-zone information are useful, but using them alone is not enough to fully capture the continuous communication demand along the predefined evacuation corridor.

Table 4 reports the sensitivity of the proposed search to different refinement radius sequences. The one-step sequence $\{170\}$ m already captures the main high-demand region, but its local adjustment capability is limited. Adding a second radius slightly improves DW-EPC. The default sequence $\{170, 75, 30\}$ m achieves nearly the same DCR and DW-EPC as the deeper sequence $\{170, 90, 45, 20\}$ m while requiring fewer recovery-utility evaluations. This indicates that the search performance is not highly sensitive to moderate changes in the refinement radius sequence provided that the sequence contains one coarse exploration radius and one or two smaller refinement radii. Further refinement mainly increases computational cost rather than recovery performance.

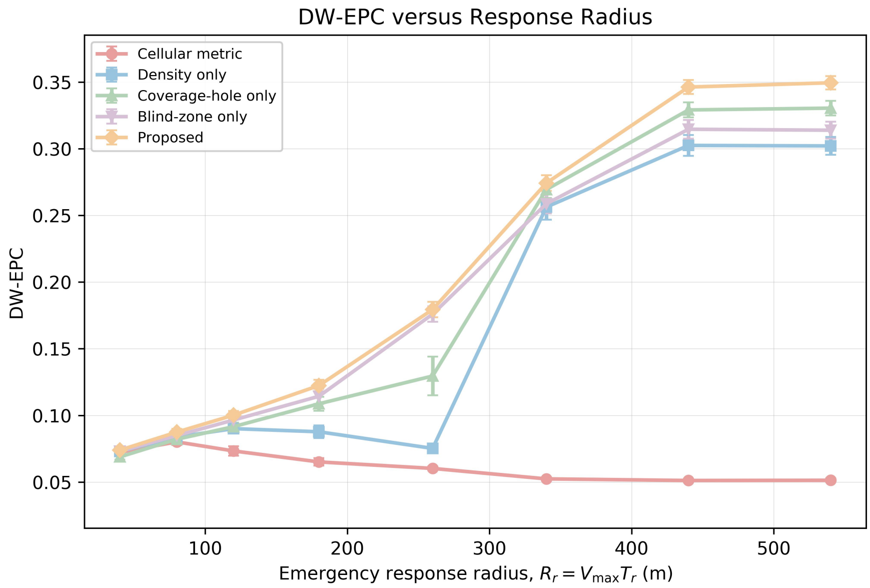

Figure 5. DW-EPC versus response radius.

Table 4. Sensitivity of the proposed search to refinement radius sequences.

Refinement Sequence $\mathcal{R}$ (m)	L	DCR	DW-EPC	Avg. Utility Evaluations
$\{170\}$	1	0.368	0.310	66.0
$\{170, 75\}$	2	0.372	0.314	112.2
$\{170, 75, 30\}$ (default)	3	0.373	0.316	161.8
$\{170, 90, 45, 20\}$	4	0.373	0.316	209.5

Figure 6 evaluates the impact of localization uncertainty in sensing outputs, denoted by σ_s, on DCR and DW-EPC. As σ_s increases, the performance of all the schemes decreases. This shows that sensing errors affect the construction of the evacuee state field and further influence UAV-BS recovery position selection.

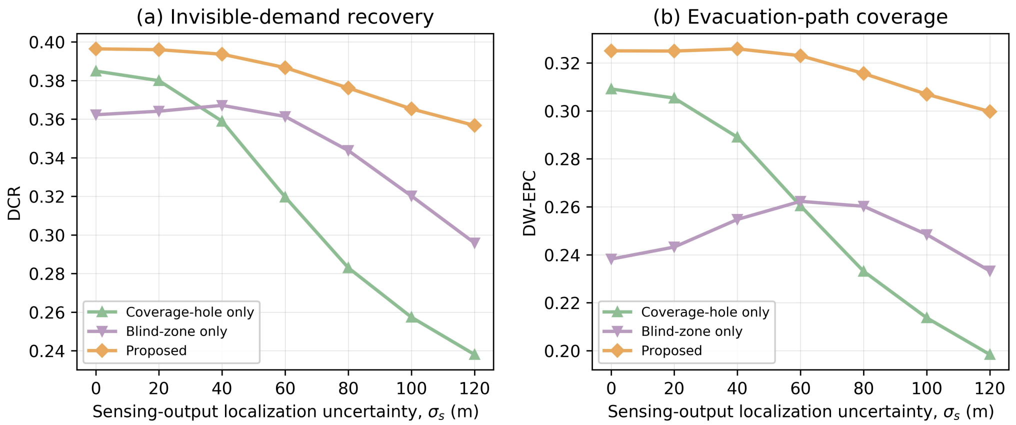

Figure 6. Robustness to localization uncertainty in sensing outputs.

Figure 6a shows that coverage-hole only suffers the largest DCR loss. This indicates that a deployment criterion based only on coverage degradation and sensed density is sensitive to sensing errors. Blind-zone only is more stable under moderate uncertainty, but it also degrades when σ_s becomes large. In contrast, the proposed scheme keeps the highest DCR over the whole uncertainty range, which indicates better robustness in invisible-demand recovery.

Figure 6b shows a similar trend for DW-EPC. The proposed scheme maintains the highest evacuation-path coverage under all the tested values of σ_s. This suggests that the joint use of D_{inv} and D_{flow} can reduce the impact of sensing uncertainty on UAV-BS recovery decisions. Therefore, the proposed criterion based on the constructed demand maps does not rely only on a single sharp sensing-density peak but also uses blind-zone information and evacuation-flow information along the corridor to guide recovery.

The robustness difference can be explained by how the two criteria use the sensing output. The blind-zone-only baseline relies mainly on the sensed density weighted by the effective blind-zone factor; as the localization uncertainty σ_s increases, the broadened sensing kernel smooths the sensed density field and weakens local density peaks, so the selected position closely follows the distorted or displaced peak. In contrast, the proposed criterion combines the invisible-demand map D_{inv} and the evacuation-flow demand map D_{flow}. Although D_{flow} still depends on the sensing output, it reweights the sensed density by corridor proximity, flow alignment, and motion intensity so that noisy peaks far from the predefined corridor or inconsistent with the evacuation direction are down-weighted while corridor-consistent demand is emphasized. This reduces the dependence on a single noisy density peak and explains the more gradual degradation of the proposed scheme observed in Figure 6.

6. Conclusions

This paper investigated UAV-BS aerial network recovery for post-disaster predefined evacuation corridors, where part of the actual communication demand may remain difficult for the damaged ground network to reliably serve or observe. To address this issue, we distinguished coverage blind zones from observation blind zones and proposed a sensing-assisted UAV-BS recovery method based on invisible-demand modeling. The proposed method converts aerial sensing outputs into an invisible-demand map and an evacuation-flow demand map, which jointly guide UAV-BS recovery position selection. Based on these maps, we developed a demand-weighted recovery criterion and a lightweight adaptive position search method for UAV-BS deployment. The simulation results show that the proposed method achieves more balanced recovery performance than methods based only on network-visible demand, sensing density, coverage degradation, or blind-zone recovery. The proposed framework improves invisible-demand coverage and evacuation-path coverage while maintaining competitive disconnected-user recovery and edge-rate performance. The results also show that the proposed method experiences smaller performance degradation than existing methods under sensing localization errors and limited UAV response ranges.

Since the current study considers a single UAV-BS with an equivalent distance-dependent SNR and no inter-UAV interference, future work will extend the method to multi-UAV cooperation with inter-UAV interference management and to multiple simultaneous evacuation corridors via priority-weighted demand maps, road-network-based evacuation corridors, rolling-horizon deployment, and real UAV platform tests that consider onboard computing limits, dynamic channels, flight stability, sensing uncertainty, and communication latency.

Author Contributions: W.Y.: conceptualization, resources, writing—review and editing, supervision, and funding acquisition. Y.L.: conceptualization, methodology, software, and writing—original draft preparation. D.W.: methodology, software, and writing—review and editing. Y.H.: conceptualization, resources, and writing—review and editing. Y.J.: formal analysis and writing—review and editing. L.L.: conceptualization, resources, writing—review and editing, supervision, project administration, and funding acquisition. All authors have read and agreed to the published version of the manuscript.

Funding: This work was supported in part by the Fundamental Research Funds for the Central Universities (No. D5000240315), the National Natural Science Foundation of China under Grant (No. 62401230), the National Key R&D Program of China (No. 2024YFC2206803 and 2024YFC2206804), and the Fund for Cultivating Practical Innovation Ability of Master's Students at Northwestern Polytechnical University (No. PF2026028).

Institutional Review Board Statement: Not applicable.

Informed Consent Statement: Not applicable.

Data Availability Statement: The original contributions presented in this study are included in the article. Further inquiries can be directed to the corresponding author.

Conflicts of Interest: The authors declare no conflicts of interest.

Abbreviations

The following abbreviations are used in this manuscript:

BS	Base Station
DCR	Demand Coverage Ratio

DRR	Disconnected-User Recovery Ratio
DW-EPC	Demand-Weighted Evacuation-Path Coverage
ISAC	Integrated Sensing and Communication
KDE	Kernel Density Estimation
RSMA	Rate-Splitting Multiple Access
SINR	Signal-to-Interference-Plus-Noise Ratio
SNR	Signal-to-Noise Ratio
UAV	Unmanned Aerial Vehicle
UAV-BS	UAV-Mounted Base Station
UAV-ISAC	UAV-Enabled Integrated Sensing and Communication

References

1. Matracia, M.; Saeed, N.; Kishk, M.A.; Alouini, M.-S. Post-Disaster Communications: Enabling Technologies, Architectures, and Open Challenges. *IEEE Open J. Commun. Soc.* **2022**, *3*, 1177–1205. [CrossRef]
2. Matracia, M.; Kishk, M.A.; Alouini, M.-S. On the Topological Aspects of UAV-Assisted Post-Disaster Wireless Communication Networks. *IEEE Commun. Mag.* **2021**, *59*, 59–64. [CrossRef]
3. Alhindi, A.; Alyami, D.; Alsubki, A.; Almousa, R.; Al Nabhan, N.; Al Islam, A.B.M.A.; Kurdi, H. Emergency Planning for UAV-Controlled Crowd Evacuations. *Appl. Sci.* **2021**, *11*, 9009. [CrossRef]
4. Shende, A.; Singh, M.P.; Kachroo, P. Optimal Feedback Flow Rates for Pedestrian Evacuation in a Network of Corridors. *IEEE Trans. Intell. Transp. Syst.* **2013**, *14*, 1053–1066. [CrossRef]
5. Huang, Z.; Fang, Z.; Ye, R.; Chraibi, M. A Matrix Translation Model for Evacuation Path Optimization. *IEEE Trans. Intell. Transp. Syst.* **2024**, *25*, 1374–1383. [CrossRef]
6. Yang, X.; Zhang, R.; Li, Y.; Pan, F. Passenger Evacuation Path Planning in Subway Station Under Multiple Fires Based on Multiobjective Robust Optimization. *IEEE Trans. Intell. Transp. Syst.* **2022**, *23*, 21915–21931. [CrossRef]
7. Matracia, M.; Kishk, M.A.; Alouini, M.-S. UAV-Aided Post-Disaster Cellular Networks: A Novel Stochastic Geometry Approach. *IEEE Trans. Veh. Technol.* **2023**, *72*, 9406–9418. [CrossRef]
8. Shah, A.F.M.S. Architecture of Emergency Communication Systems in Disasters through UAVs in 5G and Beyond. *Drones* **2023**, *7*, 25. [CrossRef]
9. Li, L.; Zhu, L.; Huang, F.; Wang, D.; Li, X.; Wu, T.; He, Y. Post-Disaster Emergency Communications Enhanced by Drones and Non-Orthogonal Multiple Access: Three-Dimensional Deployment Optimization and Spectrum Allocation. *Drones* **2024**, *8*, 63.
10. He, Y.; Huang, F.; Wang, D. PP-RCR: A Position-Probability-Resource Cooperative Routing Algorithm for Air-to-Ground Integrated Mobile Ad Hoc Networks in Emergency Rescue Scenarios. *IEEE Wirel. Commun. Lett.* 2026, *early access*. [CrossRef]
11. Danjo, A.; Hara, S.; Matsuda, T.; Ono, F.; Miura, R. 3D Determination of Message Collection and Delivery Locations for UAV-Enabled Disaster Recovery Networks. *IEEE Access* **2021**, *9*, 43533–43545. [CrossRef]
12. Citroni, R.; Mangini, F.; Frezza, F. Efficient Integration of Ultra-Low Power Techniques and Energy Harvesting in Self-Sufficient Devices: A Comprehensive Overview of Current Progress and Future Directions. *Sensors* **2024**, *24*, 4471. [CrossRef] [PubMed]
13. Zhang, T.; Lei, J.; Liu, Y.; Feng, C.; Nallanathan, A. Trajectory Optimization for UAV Emergency Communication with Limited User Equipment Energy: A Safe-DQN Approach. *IEEE Trans. Green Commun. Netw.* **2021**, *5*, 1236–1247. [CrossRef]
14. Pijnappel, T.R.; van den Berg, J.L.; Borst, S.C.; Litjens, R. Online Positioning of a Drone-Mounted Base Station in Emergency Scenarios. *IEEE Trans. Veh. Technol.* **2024**, *73*, 5572–5586. [CrossRef]
15. Al-Ahmed, S.A.; Shakir, M.Z.; Zaidi, S.A.R. Optimal 3D UAV Base Station Placement by Considering Autonomous Coverage Hole Detection, Wireless Backhaul and User Demand. *J. Commun. Netw.* **2020**, *22*, 467–475. [CrossRef]
16. Wang, Z.; Xu, L.; Hou, Y.; Wang, L.; Li, G. UAV-Assisted Emergency Integrated Sensing and Communication Networks: A CNN-Based Rapid Deployment Approach. *arXiv* **2024**, arXiv:2401.07001.
17. Liu, Y.; Mao, W.; Li, X.; Huangfu, W.; Ji, Y.; Xiao, Y. UAV-Assisted Integrated Sensing and Communication for Emergency Rescue Activities Based on Transfer Deep Reinforcement Learning. In Proceedings of the ACM MobiCom Workshop on Integrated Sensing and Communications, Washington, DC, USA, 18 November 2024.
18. Zhao, H.; Wu, M.; Wang, D.; Guizani, M.; Leung, V.C.M. Sensing-Assisted Secure Beamforming for RIS-Enabled ISAC With Leakage Suppression. *IEEE Trans. Wirel. Commun.* **2026**, *25*, 17755–17769. [CrossRef]
19. Peng, G.; Xia, Y.; Zhang, X.; Bai, L. UAV-Aided Networks for Emergency Communications in Areas with Unevenly Distributed Users. *J. Commun. Inf. Netw.* **2018**, *3*, 23–33. [CrossRef]
20. Zhang, J.; Zhou, L.; Tang, Q.; Ngai, E.C.-H.; Hu, X.; Zhao, H.; Wei, J. Stochastic Computation Offloading and Trajectory Scheduling for UAV-Assisted Mobile Edge Computing. *IEEE Internet Things J.* **2019**, *6*, 3688–3699. [CrossRef]

21. Ning, Z.; Ji, H.; Wang, X.; Ngai, E.C.-H.; Guo, L.; Liu, J. Joint Optimization of Data Acquisition and Trajectory Planning for UAV-Assisted Wireless Powered Internet of Things. *IEEE Trans. Mob. Comput.* **2025**, *24*, 1016–1030. [CrossRef]
22. He, Y.; Huang, F.; Liang, Y.; Wang, D.; Zhao, H.; Lou, J.; Zhang, R. Sum Secrecy Rate Enhancement in Low-Altitude Intelligent Networks With Mixed Obstacles. *IEEE Internet Things J.* 2026, *early access*. [CrossRef]
23. Wang, M.; Wang, D.; Zhao, H.; He, Y.; Tang, X.; Zhou, F.; Wei, Z.; Li, L. Cognitive Spectrum Sharing in Space-Air-Ground Integrated Networks: Optimizing Beamforming and AAV Trajectories With Two-Layer RSMA. *IEEE Trans. Cogn. Commun. Netw.* **2026**, *12*, 8703–8717. [CrossRef]
24. Wang, D.; Liu, T.; Li, L.; Yang, W.; Jin, Y.; Zhao, H.; He, Y.; Zhang, R. Performance Analysis of UAV–RIS-Assisted Short-Packet Secure Communications. *IEEE Internet Things J.* **2025**, *12*, 53039–53054. [CrossRef]
25. Wang, D.; Li, J.; Lv, Q.; He, Y.; Li, L.; Hua, Q.; Alfarraj, O.; Zhang, J. Integrating Reconfigurable Intelligent Surface and AAV for Enhanced Secure Transmissions in IoT-Enabled RSMA Networks. *IEEE Internet Things J.* **2025**, *12*, 9405–9419. [CrossRef]
26. Lai, C.-C.; Chen, C.-T.; Wang, L.-C. On-Demand Density-Aware UAV Base Station 3D Placement for Arbitrarily Distributed Users with Guaranteed Data Rates. *IEEE Wirel. Commun. Lett.* **2019**, *8*, 913–916. [CrossRef]
27. Zhou, Y.; Liu, X.; Zhai, X.; Zhu, Q.; Durrani, T.S. UAV-Enabled Integrated Sensing, Computing, and Communication for Internet of Things: Joint Resource Allocation and Trajectory Design. *IEEE Internet Things J.* **2024**, *11*, 12717–12727. [CrossRef]
28. Feng, J.; Liu, X.; Liu, Z.; Liu, Y. Trajectory Design and Resource Allocation for RSMA-UAV Enabled Integrated Sensing and Communication Networks. *IEEE Trans. Cogn. Commun. Netw.* **2026**, *12*, 1241–1254. [CrossRef]
29. Li, B.; Liu, J.; Mu, J.; Xiao, P.; Chen, S. UAV-Enabled Integrated Sensing and Communication in Maritime Emergency Networks. *arXiv* **2024**, arXiv:2408.14027.
30. Shende, A.; Singh, M.P.; Kachroo, P. Optimization-Based Feedback Control for Pedestrian Evacuation From an Exit Corridor. *IEEE Trans. Intell. Transp. Syst.* **2011**, *12*, 1167–1176. [CrossRef]
31. Huang, Z.; Chen, W.; Li, Q.; Luo, X.; Yuan, H.; Zhang, J. Ant Colony Evacuation Planner: An Ant Colony System With Incremental Flow Assignment for Multipath Crowd Evacuation. *IEEE Trans. Cybern.* **2021**, *51*, 5559–5572. [CrossRef] [PubMed]
32. Ibuki, K.; Kamiyama, N. Evacuation Guidance System Using UAVs of Multiple Types at Disaster. In Proceedings of the IEEE International Conference on Cyber, Physical and Social Computing (CPSCom), Copenhagen, Denmark, 19–22 August 2024; pp. 154–159.
33. Helbing, D.; Molnar, P. Social Force Model for Pedestrian Dynamics. *Phys. Rev. E* **1995**, *51*, 4282–4286. [CrossRef] [PubMed]
34. Zhou, B.; Tang, X.; Zhang, H.; Wang, X. Measuring Crowd Collectiveness. *IEEE Trans. Pattern Anal. Mach. Intell.* **2014**, *36*, 1586–1599. [CrossRef] [PubMed]
35. Adam, M.S.; Nordin, R.; Abdullah, N.F.; Abu-Samah, A.; Amodu, O.A.; Alsharif, M.H. Optimizing Disaster Response through Efficient Path Planning of Mobile Aerial Base Station with Genetic Algorithm. *Drones* **2024**, *8*, 272. [CrossRef]

https://doi.org/10.3390/drones10070507